A Novel Phase Control of Semi Bridgeless Active Rectifier for Wireless Power Transfer Applications

Erdem Asa, Kerim Colak, Mariusz Bojarski, Dariusz Czarkowski
Department of Electrical & Computer Engineering
New York University, Polytechnic School of Engineering, New York, USA
ea1145@nyu.edu, kc1353@nyu.edu, mb4496@nyu.edu, dc1677@nyu.edu

***Abstract*— A novel phase control of a semi-bridgeless active rectifier (S-BAR) is investigated in order to utilize the S-BAR in wireless energy transfer applications. The standard receiver side rectifier topology is developed by replacing rectifier lower diodes with synchronous switches controlled by a phase-shifted PWM signal. Theoretical and simulation results show that the performance of the proposed S-BAR is appropriate for resonant converters that require power control at the secondary side such as contactless energy transfer systems. To confirm the performance of the proposed converter and control, experimental results are provided for a 1 kW prototype using 3, 6, and 9 inches air gap coreless transformer, which has dimension 2.5 by 2.5 feet, with 120 V input and the output voltage range of 0 to 95 V with a maximum efficiency of 94.4%.**

Keywords—pickup circuit, phase-shift, receiver control, resonant converter, semi bridgeless active rectifier, wireless energy

I. INTRODUCTION

Wireless power transfer (WPT) is a growing technology to supply power to a variety of loads for which a physical contact is not convenient or possible. Potential applications include smartphone charging platforms [1]-[2], medical implant devices [3]-[4], and electric vehicle charging [5]-[6]. Starting from the transmitter side and ending at the receiver side, the contactless energy transfer system must be well designed and organized in order to achieve high efficiency [7]-[8]. However, a power flow control of wireless pickup systems is an unresolved issue where the control settings (frequency, phase shift, or dc link control, etc.) of the primary side cannot effectively control all the secondary side outputs. A conventional pickup wireless energy transfer system is demonstrated in Fig. 1. As seen in the figure, the system consists of two main stages: the transmitter and receiver platforms. The first stage role is to deliver energy to the second stage. The dc output voltage required by the load is provided by the second stage high-frequency rectifier and a non-isolated dc/dc converter.

Magnetic coupling, circuit parameters, and load variations cause the resonant frequency deviation in the contactless system. Thus, the output voltage of the receiver power pickup differs from its original design value. These factors cause problems for applications where a stable and constant output voltage is required. Several pickup circuit topologies, compensation strategies, and control algorithms are explored in the literature [9]-[23]. A power management for multi-pickup inductive power transfer systems is presented in [19] for materials handling applications. A new power management control approach is proposed for a parallel tuned inductive power transfer (IPT) PU circuit in that paper. Researchers in [20] have investigated a multi-pickup bidirectional inductive power transfer by a frequency controller. A two dimensional inductive power transfer system for mobile robots and a capacitively coupled contactless matrix charging platform are presented in [21]-[22]. Improved AC pickups for IPT systems are proposed in [23], which presents two IPT pickups, a parallel-tuned AC-AC and a series-tuned AC-AC pickup. However, no paper suggests any secondary side controller without an additional receiver side DC/DC controller.

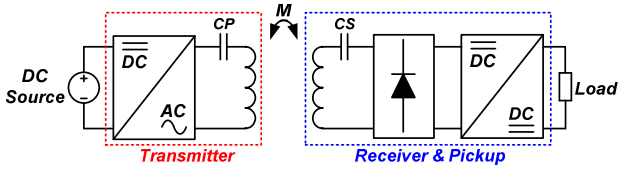

Fig. 1. A diagram of a pickup wireless energy transfer system.

In this paper, a novel phase shifted semi-bridgeless active rectifier is proposed for the wireless power transfer applications. In this topology, it is possible to control the output voltage without changing any primary side control parameters such as frequency, phase shift, etc. With this property of the circuit, especially in the multi-pickup

implementation, an independent control of each receiver ports can be achieved. In order to prove the idea and show the working principle, a single receiver port is considered in the paper. In the proposed secondary side rectifier topology S-BAR, the full bridge rectifier lower legs are replaced with synchronous rectifier (SR) switches. The SR switches are driven by a phase-shifted signal to obtain a higher voltage gain without changing the operating frequency. This novel approach results in a non-complicated pickup topology. EMI related problems can be reduced with this new approach since it provides the transmitter side control at a constant frequency. The converter model controllability is analyzed and the transfer function of the converter is derived. The system performance is confirmed with experimental results at 3, 6, and 9 inch air gaps in coreless transformer, 150 kHz operating frequency, and a 1 kW load with a maximum efficiency of 94.4% in laboratory conditions.

II. Circuit Analysis of The Wireless Power Link

In order to perform the circuit analysis, the wireless power link can be represented as two coupled inductors and two resonant capacitors connected in series as shown in Fig. 2(a). In this model, input voltage source is V_i, load impedance is $Z_{L,eq}$ where $Z_{L,eq}=\{jX_{L,eq}+R_{L,eq}\}$, two coupled inductors are L_P and L_S with equivalent series resistances R_S and R_P. K is a coupling factor between the two coils and C_P and C_S are resonant capacitors. The two coupled inductors can be equivalently modeled as a transformer with proper leakage and magnetizing inductances.

To simplify analysis, both coils L_P and L_S are assumed to be identical and equal to L. Then, the model can be equivalently represented by the circuit in Fig. 2(b). In this model $V_{i,1}$ is a fundamental component of voltage source V_i, $Z_{P,eq}$ and $Z_{S,eq}$ are equivalent values where $Z_{P,eq}=\{1/j\omega C_P+j\omega L_L+R_P\}$, $Z_{S,eq}=\{1/j\omega C_S+j\omega L_L+R_S\}$. Z_M is the magnetizing impedance related to the coupled inductors by $Z_M=j\omega L_M$.

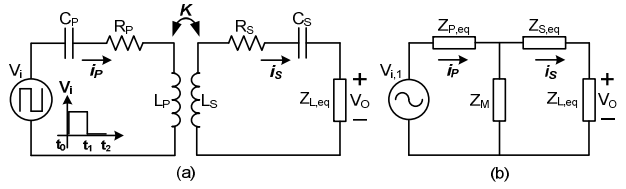

Fig. 2. Schematics of wireless power link (a) equivalent circuit model, (b) simplified model.

The model of Fig. 2(b) is related to the model of Fig. 2(a) by the following equations.

$$\begin{aligned} L_M &= K\sqrt{L_P L_S} = KL \\ L_L &= L - L_M = (1-K)L \end{aligned} \tag{1}$$

The resonant tank square wave voltage v_i is positive during the first cycle of *[t0, t1]*, and during the other cycle *[t1, t2]* is zero. Thus, $v_i(t)$ can be stated using Fourier analysis as

$$\begin{aligned} v_i(t) &= \begin{cases} V_i, & t_0 < \omega t < t_1 \\ 0, & t_1 < \omega t < t_2 \end{cases} \\ v_i(t) &= \frac{2V_i}{\pi}\sum_{n=1,3,..}^{\infty}\frac{1}{n}\sin(n\omega_{sw}t) \end{aligned} \tag{2}$$

The amplitude of the real voltage of the fundamental component of v_i and V_i are

$$v_{i,1} = \frac{2V_i}{\pi}\sin(\omega_{sw}t), \quad V_{i,1} = \frac{2V_i}{\pi} \tag{3}$$

Neglecting parasitic resistances R_P, R_S, and using the Kirchhoff's voltage law, transmitter and receiver resonant tank in a matrix form is

$$\begin{bmatrix} V_{i,1} \\ 0 \end{bmatrix} = \begin{bmatrix} \frac{1}{j\omega C_P} + j\omega L_P & -j\omega L_M \\ -j\omega L_M & \frac{1}{j\omega C_P} + j\omega L_P + jX_{L,eq} + R_{L,eq} \end{bmatrix} \begin{bmatrix} I_P \\ I_S \end{bmatrix} \tag{4}$$

The proposed system theoretical analysis is simplified using the fundamental component approximation (FHA) method. Transformer primary side reflected AC equivalent impedance can be stated in CCM and DCM mode.

$$\begin{aligned} Z_{L,eq} &= \frac{4}{\pi^2}R_L(1-\cos\beta)\sin\left(\frac{\beta}{2}\right)e^{j[\pi/2-\beta/2]} \quad ,\Theta > 0 \\ Z_{L,eq} &= \frac{4}{\pi^2}R_L(1-\cos\beta)\sin\left(\frac{\beta}{2}\right)e^{j[\beta/2-\pi/2]} \quad ,\Theta < 0 \end{aligned} \tag{5}$$

where Θ is positive or negative sign of receiver voltage and current phase difference that indicates the load is inductive or capacitive; the reflected impedance to the receiver is shown as an inductive $\Theta>0$, and as a capacitive $\Theta<0$. Taking real and imaginary portions of (5), the equivalent resistance and reactance values are obtained for the inductive load and capacitive load by the following equations.

For the inductive load:

$$\begin{aligned} R_{L,eq} &= \mathrm{Re}\left\{\frac{4}{\pi^2}R_L(1-\cos\beta)\sin\left(\frac{\beta}{2}\right)e^{j[\pi/2-\beta/2]}\right\} \quad 0 \le \beta \le \pi \\ X_{L,eq} &= \mathrm{Im}\left\{\frac{4}{\pi^2}R_L(1-\cos\beta)\sin\left(\frac{\beta}{2}\right)e^{j[\pi/2-\beta/2]}\right\} \quad 0 \le \beta \le \pi \end{aligned} \tag{6}$$

For the capacitive load:

$$R_{L,eq}=\mathrm{Re}\left\{\frac{4}{\pi^2}R_L(1-\cos\beta)\sin\left(\frac{\beta}{2}\right)e^{j[\beta/2-\pi/2]}\right\}\quad \pi\le\beta\le 2\pi$$
$$X_{L,eq}=\mathrm{Im}\left\{\frac{4}{\pi^2}R_L(1-\cos\beta)\sin\left(\frac{\beta}{2}\right)e^{j[\beta/2-\pi/2]}\right\}\quad \pi\le\beta\le 2\pi \tag{7}$$

Normalized parameters help to find the transfer function of the system using design parameter values. These equations are defined and explained as follows.

$$\omega_R=\frac{1}{\sqrt{L_P C_P}},\quad Z_O=\sqrt{\frac{L_P}{C_P}},\quad Q=\frac{R_{L,eq}}{Z_O},\quad \omega_N=\frac{\omega_{sw}}{\omega_R} \tag{8}$$

where ω_R is the resonant frequency. Characteristic impedance Z_O affects the operating frequency range of the system. The quality factor Q is defined as the ratio of the total average stored energy and the dissipated energy per cycle. The normalized frequency ω_N depends on the switching ω_{sw} and resonant frequency ω_R. The voltage transfer function of the system is deduced in (9) shown at the bottom of the page.

This gain function reveals the characteristic of the system under frequency and phase shift angle changes. The boundary conditions are such that the gain should be selected low enough under the maximum frequency at the minimum output voltage, and high enough under the minimum frequency at the maximum output voltage. The required maximum voltage gain can be expressed as $M_{V,max}=V_{out,max}/V_{in}$ and $M_{V,min}=V_{out,min}/V_{in}$ to form the boundary.

III. Analysis Of The Proposed Converter

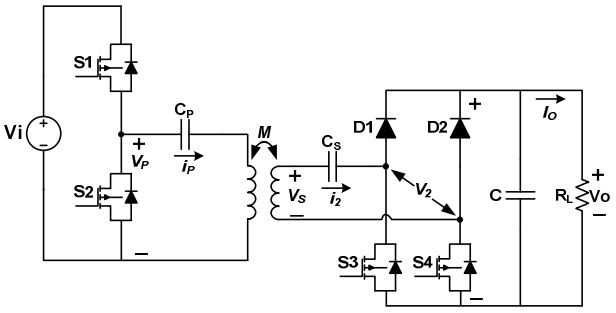

Fig. 3. The proposed phase controlled of S-BAR.

The proposed phase-control principle of a semi bridgeless active rectifier (S-BAR) circuit topology for the wireless power transfer is shown in Fig. 3. It comprises a half bridge resonant inverter, an air gap coreless transformer, and a single-phase semi-bridge rectifier in the secondary side. The active rectifier is comprised of two transistors with anti-parallel diodes in the lower part of switching legs and two diodes in the upper parts [24]. The phase-shift angle of the secondary side transistors regulates the output voltage and power in the load.

The operating waveforms and switch state transitions are presented in Figs. 4 and 5 to show the behavior of the proposed converter. To simplify the circuit analysis, secondary side rectifier diodes and switches are ideal, the output capacitor is assumed to be large enough for a constant dc output, and filter losses are neglected. The proposed circuit is examined under these conditions in the following operation modes:

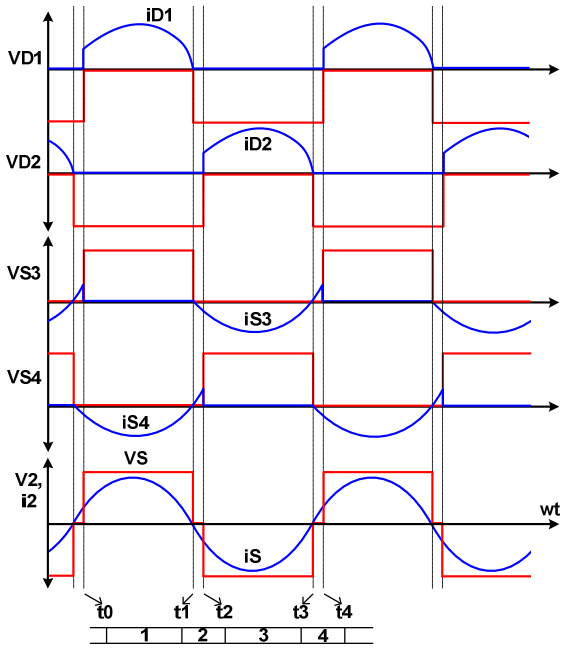

Fig. 4. Voltage and current waveforms in the switch and diodes.

Mode 1 [t0<t<t1]

During this interval, the rectifier switch S_4 is turned on and diode D_1 is in on-state. As shown in Fig. 4, the cycle starts with positive current i_S and the current flows through D_1, and S_4 in the converter as depicted in Fig. 5(a).

Mode 2 [t1<t<t2]

The current flows in negative direction in this mode through switches S_3 and S_4 as shown in Fig. 5(b). Both diodes are negative biased and secondary side is shorted with switches S_3 and S_4. The current wave is demonstrated in Fig. 4.

$$M_V=\frac{\left(R_{L,eq}+jX_{L,eq}\right)j\omega_N K Z_O}{\frac{\left(1-\omega_N(1-K)\right)Z_O}{\left(1-\omega_N^2\right)}-\frac{\left(1-\omega_N(1-K)\right)Z_O^2\left(1-\omega_N^2\right)}{\omega_N^2}+\frac{\left(1-\omega_N^2\right)\left(R_{L,eq}+jX_{L,eq}\right)}{j\omega_N}} \tag{9}$$

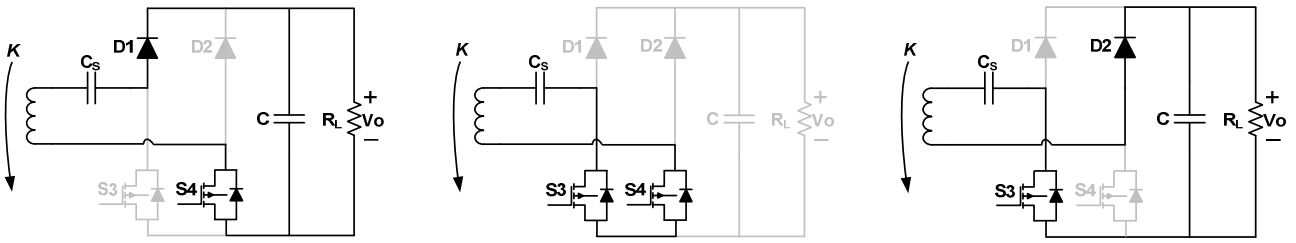

(a) Mode 1 (b) Mode 2 and Mode 4 (c) Mode 3

Fig. 5. Mode analysis, current path and switching transition in the receiver side.

Mode 3 [t2<t<t3]

The resonant current further decreases in this interval and reaches the minimum value within this mode as plotted in Fig. 4. The switch S_3 is on, while diode D_1 is off and D_2 is in the on state. The current flows from the coreless transformer to the receiver side switch S_3 and diode D_2 as shown in Fig. 5(c).

Mode 4 [t3<t<t4]

The current flows in positive direction in the resonant tank, and the receiver side switches S_3 and S_4 are shorted as shown in Fig. 5(b). Both diodes are reverse biased and S_3, S_4 are in the conduction mode. The current wave is demonstrated in Fig. 4. After this interval, the modes are completed and the inverter continues with Mode 1 again.

IV. The Phase Shift Control

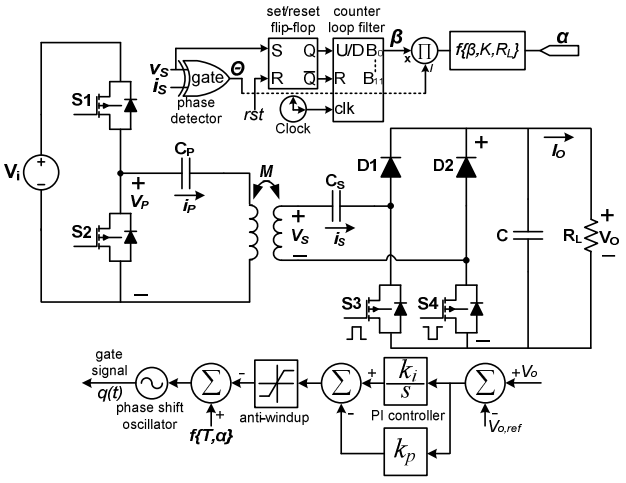

Fig. 6. The phase controlled of S-BAR converter.

Due to small complexity of the S-BAR converter, the control of the system is relatively simpler than utilization of communication devices for the misalignment or position/distance determination and additional dc/dc converter stages in the receiver side. In this proposed approach, the receiver side can be controlled without the need for the transmitter side. Only voltage and current signals at the receiver inputs and voltage sensing at the output are sufficient to control the system by generating two phase-shifted PWM pulses.

The proposed phase shift approach to the S-BAR control is shown in Fig. 6. The designed control is implemented in FPGA and a microprocessor. The system operating frequency *(1/T)*, phase difference detection between receivers input voltage and current Θ, and secondary side rectifier conduction angle β are determined by an FPGA block. Also, high voltage, current, and temperature protection are ensured by FPGA. The control angle α estimation is carried by a microprocessor with β, coupling coefficient factor K, and load R_L as parameters and considering voltage and current phase detection Θ to use the right set of equations (inductive or capacitive load). For the system control, α determination is important to manage the output at the load terminals.

V. Experimental Results

The proposed wireless system is designed for 1 kW, 120 V input voltage, and 0-95 V output voltage rating as a laboratory prototype. The coreless transformer is tested with 3, 6, and 9 inch distances between coils which results in 0.5, 0.33, and 0.25 coupling factor respectively. The topology parameters of the converter are given in Table I.

TABLE I

Symbol	Parameter	Value
V_i	dc input voltage	120 V
V_O	dc output voltage range	0-95 V
I_O	dc output current	10 A
P_O	maximum output power	1 kW
C_P, C_S	resonant capacitors	40 nF
L_P, L_S	coil self-inductances	25 uH
d	square coil dimension	2.5 x 2.5 feet
n	coil turn number	4
f_{SW}	operating frequency	150 kHz

The characteristic waveforms of the proposed converter described in section III and IV are given to verify circuit operation. Selected current and voltage waveforms at different control angles with different coupling factors are given in Fig. 7. The phase-shift angle controls the output voltage by

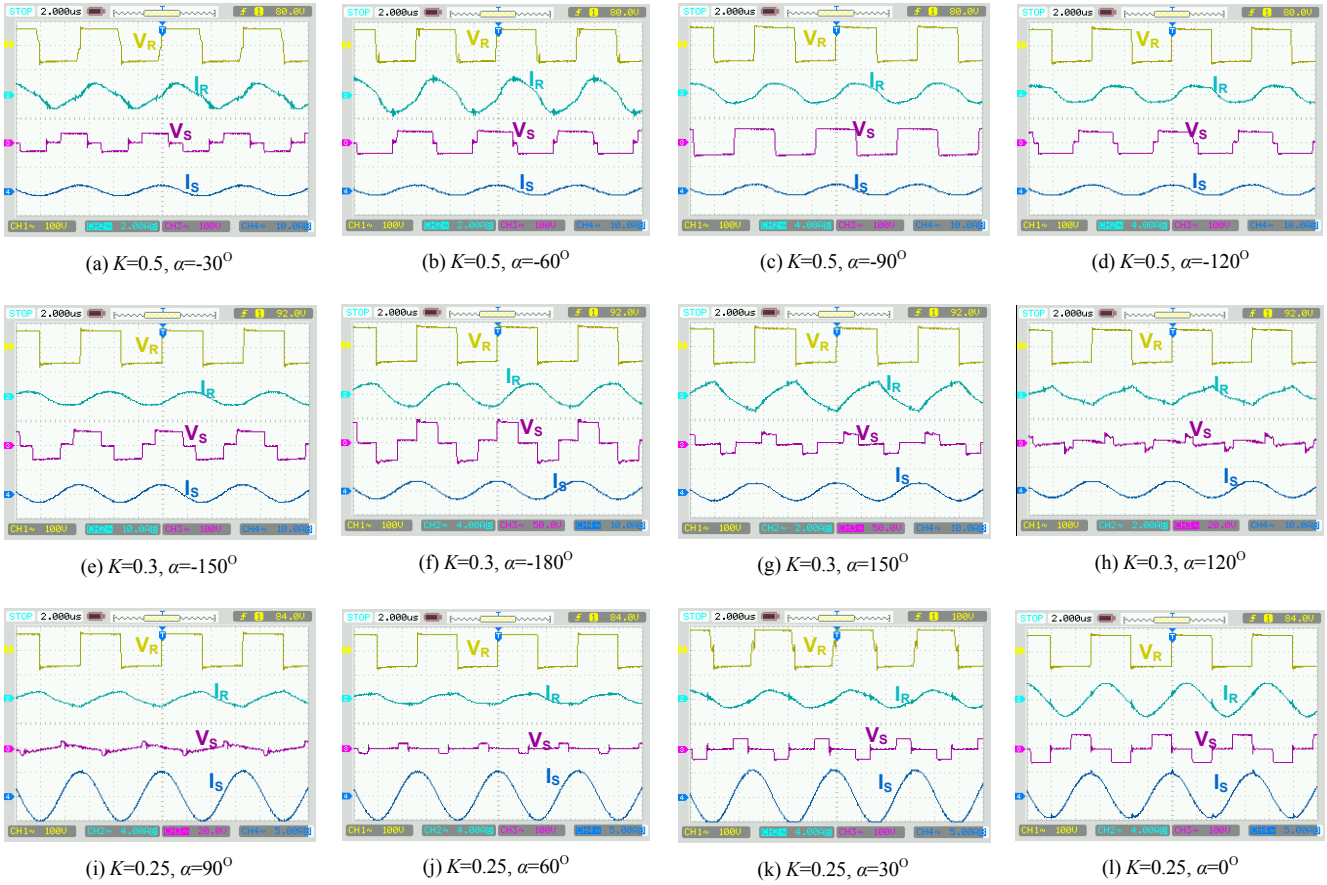

(a) K=0.5, α=-30^O (b) K=0.5, α=-60^O (c) K=0.5, α=-90^O (d) K=0.5, α=-120^O

(e) K=0.3, α=-150^O (f) K=0.3, α=-180^O (g) K=0.3, α=150^O (h) K=0.3, α=120^O

(i) K=0.25, α=90^O (j) K=0.25, α=60^O (k) K=0.25, α=30^O (l) K=0.25, α=0^O

Fig. 7. Resonant tank voltage V_R, current I_R and secondary side voltage V_S, current I_S waveforms with different coupling coefficients K and phase shift control angle α.

changing the transformer secondary side voltage as shown in the figure.

Fig. 8 shows the output voltage characteristics versus the phase shift angle with different K values. When the switching frequency is constant at 150 kHz, the phase shift angle is swept to obtain the output voltage waveform at each different K. As seen in the figure, the output voltage changes in two regions when the phase shift angle is lower than zero in the first region $(\alpha<0)$ and greater than zero $(\alpha>0)$ in the second region. The wide output voltage range 0 to 45 V, 0 to 70 V, and 0 to 95 V can be achieved in these two regions.

The efficiency characteristics of the proposed topology versus the phase shift angle with different K are given in Fig. 9. The efficiency of the converter is greater than 80 % in all different couplings when the phase shift is $\alpha<0$. It reaches the maximum efficiency 94.4% at 0.5 coupling with the phase shift angle around -90 degrees. Considering the output voltage characteristic at the constant load in the experimental results, the variable voltage range of 25 to 45 V, 40 to 70 V, and 50 to 95 V can be achieved with a high efficiency for $\alpha<0$. Operation at $\alpha>0$ yields low efficiency and should be avoided because of the high circulating current and hard switching conditions.

VI. Conclusions

In this study, a new phase control of a semi-bridgeless active rectifier (S-BAR) is presented for wireless power transfer applications. The simple converter topology has reduced number of switches on the secondary side comparing to typical inductive energy transfer secondary side dc/dc converter topologies. The converter model analysis with steady state equivalent circuits is given using FHA and voltage/current waveforms are displayed in all operating modes. The transfer function of the converter is derived analytically. The proposed control adjusts the output voltage of the system by phase shift tuning of the active switches in the receiver. The concepts presented here can be also used in multiple output receiver wireless applications since the output control can be regulated only in the receiver side. The system performance is confirmed with theoretical and experimental results at various coupling coefficient factors. To verify the proposed phase shifted S-BAR converter, a 1 kW full power

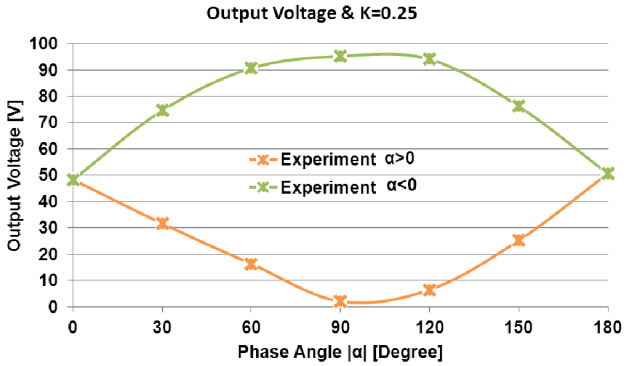

(a)

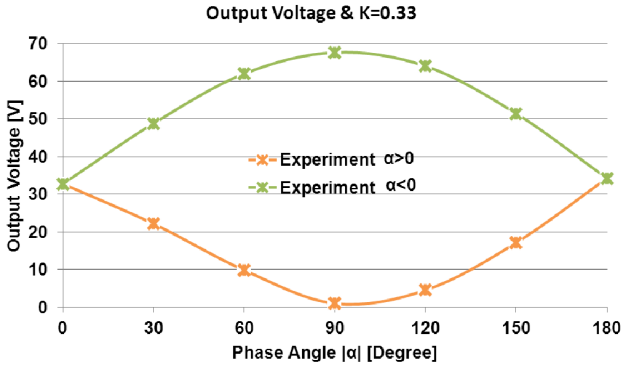

(b)

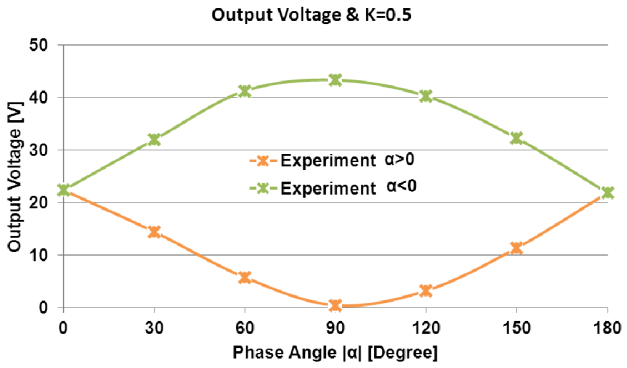

(c)

Fig. 8. Comparison of measured and calculated power as a function of the control phase angle with different *K's*; (a) *K*=0.25, (b) *K*=0.33, (c) *K*=0.5.

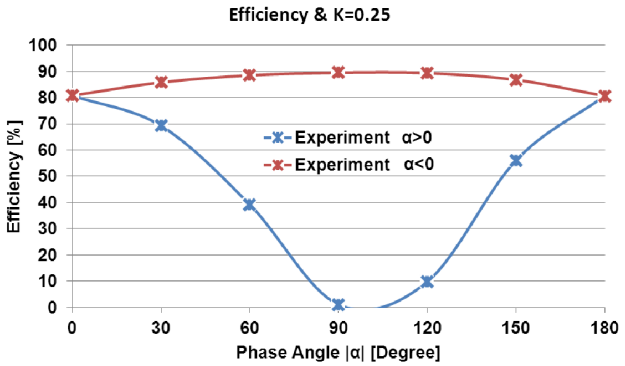

(a)

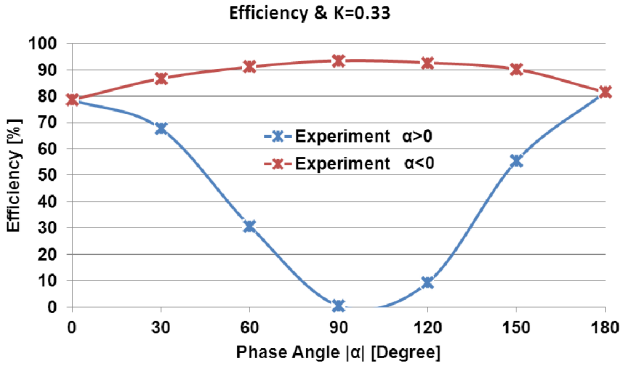

(b)

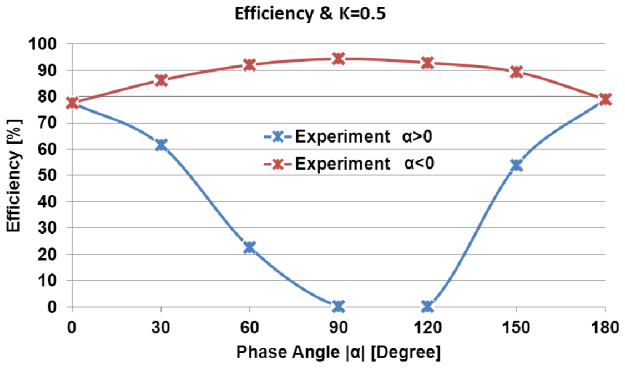

(c)

Fig. 9. Comparison of measured and calculated effficiency as a function of the control phase angle with different *K's*; (a) *K*=0.25, (b) *K*=0.33, (c) *K*=0.5.

prototype is designed at 120 V input. The laboratory prototype achieved a 94.4% maximum efficiency.

REFERENCES

[1] Y. Jang, M. M. Jovanovic, "A Contactless Electrical Energy Transmission System for Portable Telephone Battery Chargers," IEEE Transactions on Industrial Electronics, vol.50, no.3, pp.520527, June 2003.

[2] K. C. Wan, Q. Xue, X. Liu, S. Y. Hui, "Passive Radio Frequency Repeater for Enhancing Signal Reception and Transmission in a Wireless Charging Platform," IEEE Transactions on Industrial Electronics, vol.61, no.4, pp.17501757, April 2014.

[3] A. K. RamRakhyani, G. Lazzi, "On the Design of Efficient Multi Coil Telemetry System for Biomedical Implants," IEEE Transactions on Biomedical Circuits and Systems, vol.7, no.1, pp.1123, February 2013.

[4] M. Q. Nguyen, Z. Hughes, P. Woods, Y. S. Seo; S. Rao, J. C. Chiao, "Field Distribution Models of Spiral Coil for Misalignment Analysis in Wireless Power Transfer Systems," IEEE Transactions on Microwave Theory and Techniques, vol.62, no.4, pp.920930, April 2014.

[5] U. K. Madawala, M. Neath, D. J. Thrimawithana, "A Power Frequency Controller for Bidirectional Inductive Power Transfer Systems," IEEE Transactions on Industrial Electronics, vol.60, no.1, pp.310317, January 2013.

[6] F. Musavi, W. Eberle, "Overview of Wireless Power Transfer Technologies for Electric Vehicle Battery Charging," IET Power Electronics, vol.7, no.1, pp.6066, January 2014.

[7] W. Zhang, S. C. Wong, C. K. Tse, Q. Chen, "Design for Efficiency Optimization and Voltage Controllability of Series Series Compensated Inductive Power Transfer Systems," IEEE Transactions on Power Electronics, vol.29, no.1, pp.191200, January 2014.

[8] C. Florian, F. Mastri, R. P. Paganelli, D. Masotti, A. Costanzo, "Theoretical and Numerical Design of a Wireless Power Transmission Link With GaN Based Transmitter and Adaptive Receiver," IEEE Transactions on Microwave Theory and Techniques, vol.62, no.4, pp.931946, April 2014.

[9] W. Zhang, S. Wong, C. Tse, Q. Chen, "An Optimized Track Length in Roadway Inductive Power Transfer Systems," IEEE Journal of Emerging and Selected Topics in Power Electronics, in press.

[10] J. Huh, S. W. Lee, W. Y. Lee, G. H. Cho, C. T. Rim, "Narrow-Width Inductive Power Transfer System for Online Electrical Vehicles," IEEE Transactions on Power Electronics, vol.26, no.12, pp.36663679, December 2011.

[11] G. Elliott, S. Raabe, G. A. Covic, J. T. Boys, "Multiphase Pickups for Large Lateral Tolerance Contactless Power-Transfer Systems," IEEE Transactions on Industrial Electronics, vol.57, no.5, pp.15901598, May 2010.

[12] G. A. Covic, J. T. Boys, A. M. W. Tam, J. C. H. Peng, "Self Tuning Pick-ups for Inductive Power Transfer," IEEE Power Electronics Specialists Conference (PESC), pp.3489,3494, June 2008.

[13] P. Si; A. P. Hu, S. Malpas, D. Budgett, "Switching Frequency Analysis of Dynamically Detuned ICPT Power Pick-ups," International Conference on Power System Technology (PowerCon), pp.18, October 2006.

[14] J. U. W. Hsu, A. P. Hu, A. Swain, "A Wireless Power Pickup Based on Directional Tuning Control of Magnetic Amplifier," IEEE Transactions on Industrial Electronics, vol.56, no.7, pp.2771,2781, July 2009.

[15] Z. Pantic, S. M. Lukic, "Framework and Topology for Active Tuning of Parallel Compensated Receivers in Power Transfer Systems," IEEE Transactions on Power Electronics, vol.27, no.11, pp.45034513, November 2012.

[16] H. H. Wu, G. A. Covic, J. T. Boys, D. J. Robertson, "A Series Tuned Inductive Power Transfer Pickup With a Controllable AC Voltage Output," IEEE Transactions on Power Electronics, vol.26, no.1, pp.98-109, January 2011.

[17] U. K. Madawala, M. Neath, D. J. Thrimawithana, "A Power Frequency Controller for Bidirectional Inductive Power Transfer Systems," IEEE Transactions on Industrial Electronics, vol.60, no.1, pp.310317, January 2013.

[18] D. J. Thrimawithana, U. K. Madawala, M. Neath, "A Synchronization Technique for Bidirectional IPT Systems," IEEE Transactions on Industrial Electronics, vol.60, no.1, pp.301309, January 2013.

[19] L. Chen, J. Boys, G. Covic, "Power Management for Multiple-pickup IPT Systems in Materials Handling Applications," IEEE Journal of Emerging and Selected Topics in Power Electronics, in press.

[20] A. K. Swain, S. Devarakonda, U. K. Madawala, "Modeling, Sensitivity Analysis, and Controller Synthesis of Multipickup Bidirectional Inductive Power Transfer Systems," IEEE Transactions on Industrial Informatics, vol.10, no.2, pp.13721380, May 2014.

[21] C. Park, S. Lee, G. H. Cho, S. Y. Choi, C. T. Rim, "Two-Dimensional Inductive Power Transfer System for Mobile Robots Using Evenly Displaced Multiple Pickups," IEEE Transactions on Industry Applications, vol.50, no.1, pp.558565, February 2014.

[22] C. Liu, A. P. Hu, B. Wang, N. C. Nair, "A Capacitively Coupled Contactless Matrix Charging Platform With Soft Switched Transformer Control," IEEE Transactions on Industrial Electronics, vol.60, no.1, pp.249260, January 2013.

[23] J. E. James, D. R. Robertson, G. A. Covic, "Improved AC Pickups for IPT Systems," IEEE Transactions on Power Electronics, in press.

[24] K. Colak, E. Asa, M. Bojarski, D. Czarkowski, "A Novel LLC Resonant Converter with Semi Bridgeless Active Rectifier," IEEE Transportation Electrification Conference and Expo (ITEC), pp.16, June 2014.